Time-resolved X-ray study of poly(aryl ether ether ketone) crystallization and melting behaviour: 2. Melting

Benjamin S. Hsiao*†, KennCorwin H. Gardner‡ and Dan Q. Wu§
DuPont Company, Experimental Station, Wilmington, DE 19880, USA

and Benjamin Chu
Department of Chemistry, State University of New York at Stony Brook, Long Island, NY 11794-3400, USA
(Received 22 January 1993)

Heating measurements of amorphous and isothermally crystallized (260–320°C) samples were carried out using time-resolved small-angle X-ray scattering (SAXS) to study the melting behaviour of poly(aryl ether ether ketone) (PEEK). In the amorphous sample, the scattering maximum became detectable after the cold crystallization, with the peak position q_{max} decreasing with temperature. The latter was also seen in crystallized samples. Two types of long period (L_B and L_C^M) were determined, by using Bragg's law and the correlation function, respectively. These values are inversely proportional to q_{max}, and therefore they all increased with temperature. In the crystallized samples, two stages of increase in the long period were found: below the lower melting temperature of the double endotherms (T_{m_l}, determined by d.s.c.), the increase was small, while above T_{m_l}, both of the long periods increased rapidly. In addition, the invariant Q was found to increase with temperature but reached a maximum near the onset temperature of the last endotherm. These results were consistent with the hypothesis of sequential melting of lamellar bundles consisting of two populations of thickness. In the crystalline specimens, the increase in Q was mainly due to the thermal expansion, whereas in the amorphous sample, the larger increase in Q was additionally attributed to the broad cold crystallization.

(Keywords: SAXS; double-melting behaviour; PEEK)

INTRODUCTION

Previously, we have studied the crystallization behaviour of poly(aryl ether ether ketone) (PEEK), using time-resolved small-angle X-ray scattering (SAXS) and thermal analysis methods[1]. This is a continuation of that work, and deals with the melting aspects of PEEK. Our goals are three-fold: (1) to examine the evolution of lamellar morphology during heating of amorphous and isothermally crystallized (at different temperatures) samples; (2) to investigate the origin of the double-melting behaviour as seen by d.s.c. in crystallized samples and; (3) to verify the hypothesis of the dual-lamellar thickness model for isothermal crystallization.

It is known that many processes may take place sequentially during the heating of an amorphous PEEK specimen. First, the material will crystallize at temperatures above the glass transition temperature; this process is referred to as cold crystallization. Crystallization of this type usually covers a wide range of temperatures and therefore results in a broad distribution of lamellar thickness. By increasing the temperature, the lamellar morphology can be altered: thinner lamellae will melt away first, to leave behind the thicker lamellae, which can continue to be thickened until the temperature is high enough to destroy all crystalline entities. Such a process has been investigated using time-resolved SAXS/wide-angle X-ray diffraction (WAXD) techniques in the poly(ethylene naphthalene dicarboxylate) (PEN) system by Zachmann and co-workers[2].

Typical d.s.c. scans of isothermally crystallized PEEK samples always exhibit two melting endotherms during the heating cycle (the so-called double-melting behaviour)[3–8]. This behaviour has also been found in many semicrystalline polymers, including, among others, poly(ethylene terephthalate) (PET)[9,10], poly(butylene terephthalate) (PBT)[11], and poly(aryl ether ketone ketone) (PEKK)[12]. This type of behaviour exhibits the following features: a lower-temperature endotherm often occurs approximately 10°C above the crystallization (or annealing) temperature, whereas the higher-temperature endotherm (regarded as the nominal melting endotherm) is relatively insensitive to the crystallization temperature. The enthalpy change associated with the former endotherm is considerably less than that of the higher-temperature endotherm, but it increases slightly with both the crystallization temperature and the time. Although the origin of this double-melting behaviour is still unclear, it was shown, however, that the existence of two endotherms is not due to any changes in crystal structure. Two

* To whom correspondence should be addressed
† DuPont Fibers
‡ DuPont Central Research and Development
§ DuPont Polymers

0032-3861/93/193996-08
© 1993 Butterworth-Heinemann Ltd.

separate hypotheses have been proposed to explain this phenomenon: (1) the two endotherms are due to the melting of two distinct morphologies[4,7,9,10,13] and; (2) the endotherms are due to a melting and recrystallization process of the primary crystal morphology as a characteristic of the previous crystallization history[6,14,15]. Since both hypotheses were based on results obtained from measurements such as thermal analysis, electron microscopy and conventional X-ray diffraction/scattering of quenched samples, it was not possible to confirm which mechanism is more valid. By using the time-resolved synchrotron SAXS/WAXD technique, we hoped to be able to verify the correct mechanism for this double-melting behaviour.

In our previous work[1], we have argued that during isothermal crystallization, a lamellar insertion process can take place within the lamellar stacks. The inserted secondary lamellae may suffer from some spatial restrictions within the stacks and thus result in a narrower thickness. In this case, upon heating, the narrower lamellar thickness should melt away first, leaving behind the thicker primary lamellae, which will inevitably result in a progressive increase in the long period. This process is expected to be a function of the sample morphology. Therefore, we have prepared specimens crystallized at different temperatures in order to alter the morphology. With respect to lamellar information, we have used the correlation function $\gamma(r)$ of a random two-phase model[16] to analyse the scattering results. Although this model may be insufficient to describe a bi-model distribution of the lamellar thicknesses, we feel that the scattering intensity contributed to the secondary lamellar population is comparatively small. Therefore, the use of the two-phase model may still yield an 'average' estimation of the lamellar variables of the primary lamellae.

EXPERIMENTAL

Sample preparation

Two types of specimens of commercially available PEEK (150G, from ICI) were prepared, i.e. amorphous and crystalline. The amorphous sample was obtained by quenching the melt (from 400°C) with a cold press (quench rate is ~ 300°C min^{-1}). The crystalline specimen was prepared in a dual-chamber temperature-jump device[17] by using the following procedure. All samples were first moulded into void-free discs (with diameter and thickness of 6.75 and 1.1 mm, respectively), and the latter were then equilibrated in the high-temperature chamber (at 400°C). They were subsequently 'jumped' to the low-temperature chamber for full crystallization (annealed for 1 h). Seven crystallization temperatures were chosen over the range from 260 to 320°C, at intervals of 10°C.

Thermal analysis and time-resolved SAXS

A TA (Thermal Analysis) DSC-900 instrument was used to characterize the melting behaviour of different samples. All scans were made at a heating rate of 10°C min^{-1} under a nitrogen atmosphere. The melting temperature was taken at the peak temperature of the endotherm.

Time-resolved SAXS measurements were carried out at the X3A2 SUNY beamline, National Synchrotron Light Source, Brookhaven National Laboratory. A detailed description of the experimental set-up and the data analysis procedure has been given in the previous paper[1] in this series and elsewhere[17,18]. In this present work, specimens were heated at a rate of 10°C min^{-1} (i.e. at the same rate as used in the d.s.c.) studies, from 152 to 332°C using the dual-chamber temperature-jump apparatus. The SAXS profile was collected for 10 s, at temperature intervals of ~ 10°C, using modified Kratky optics[19] and a linear position sensitive detector. The scattering data were corrected for background, sample absorption, incident beam fluctuation, and then were smoothed by a filtering program to enhance the signal-to-noise ratio.

The scattering intensity was further corrected for local electron-density fluctuation, and truncation effects (at low and high q values), in order to calculate the correlation function $\gamma(r)$[20]. This function is defined as:

$$\gamma(r) = (1/2\pi^2) \int_0^\infty Iq^2 \cos(qr)\, dq \qquad (1)$$

where I is the corrected intensity (without taking into account the diffuse interface) and q is defined as $4\pi \sin(\theta)/\lambda$. The extension of intensity to $q = \infty$ was made by applying Porod's law. Two types of long period (L_B and L_M^C) were determined from the Lorentz-corrected plot (Iq^2 vs. q), and $\gamma(r)$, respectively. The linear degree of crystallinity x_{CL} and the invariant Q were also determined from $\gamma(r)$. The lamellar thickness l_C was calculated as the product of L_C^M and x_{CL}.

RESULTS

Amorphous specimens

A d.s.c. heating scan (at a rate of 10°C min^{-1}) of an amorphous PEEK specimen is illustrated in *Figure 1*, which shows a glass transition temperature (T_g) of 140°C, a cold crystallization temperature (T_c) of 169°C and a melting temperature (T_m) of 345°C. The enthalpy change associated with the crystallization endotherm was about the same as that of the melting endotherm, which indicated that the specimen was amorphous. The corresponding unsmoothed synchrotron SAXS patterns, collected at various selected temperatures during heating of the amorphous sample (at a rate of 10°C min^{-1}, i.e.

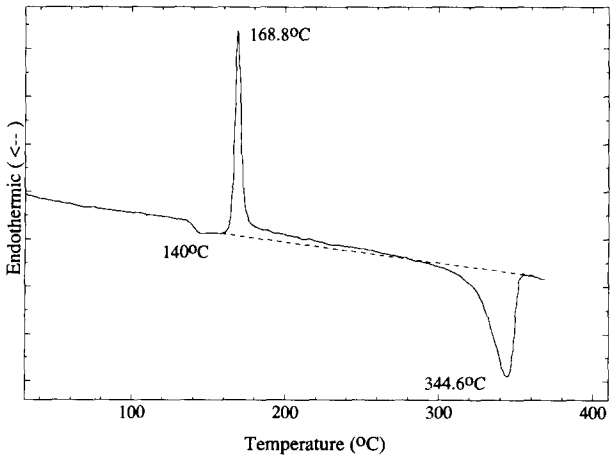

Figure 1 D.s.c. scan of an amorphous PEEK sample; the heating rate is 10°C min^{-1}

the same as for the d.s.c. measurements) are shown in *Figure 2*. It was seen that the scattering maximum was shifted to a lower pixel value (or a lower scattering angle, as the pixel number was proportional to the scattering angle) with the increase in temperature. In *Figure 2*, the scattering maximum was developed only at temperatures above T_c; below this temperature, no scattering maximum could be seen (e.g. as in the 144°C profile). At 172°C, the SAXS profile showed a 'borderline' scattering maximum. Although this scattering intensity was low and diffuse, the profile appeared to have more than one maximum. At higher temperatures, a single scattering maximum was always observed. An interesting observation was made in connection with these measurements, i.e. the signal-to-noise ratio in all of the SAXS profiles was about constant. In other words, at higher temperatures, although the SAXS intensity was larger, so also was the noise span.

Selected (Iq^2 vs. q) plots (Lorentz-corrected) of the corrected and smoothed SAXS profiles (from *Figure 2*) measured at different temperatures are shown in *Figure 3*. It was seen that the 172°C profile exhibited a peak at 0.54 nm^{-1} and two weak secondary shoulders at 0.4 and 0.24 nm^{-1}. Since this type of plot emphasizes the scattering signal at *high* values of q, the observation of these two weak shoulders (at *low* values of q) suggested

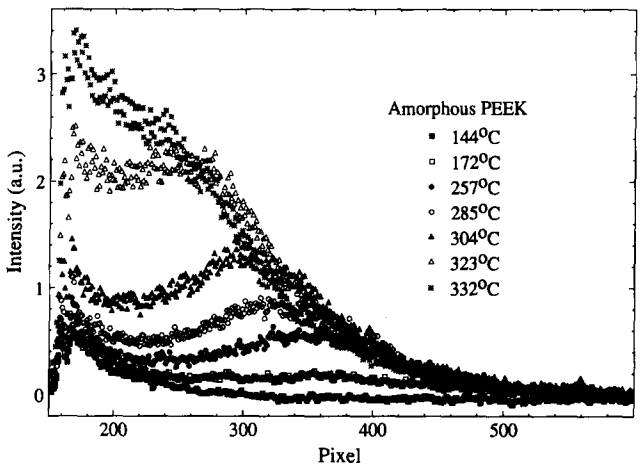

Figure 2 Unsmoothed SAXS profiles collected at different temperatures during the heating of an amorphous PEEK sample; the heating rate is 10°C min^{-1} and data collection time is 10 s

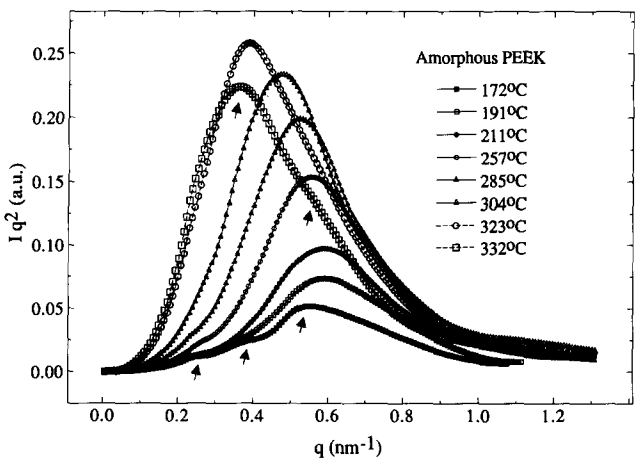

Figure 3 Lorentz-corrected SAXS profiles of the data from *Figure 2*; some selected multiple scattering peaks are indicated by arrows

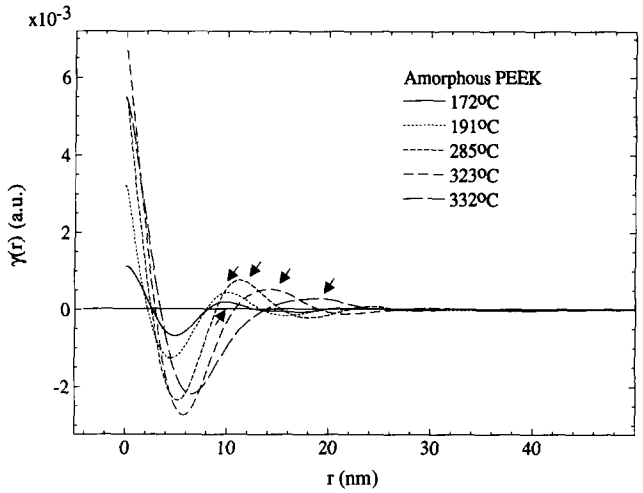

Figure 4 Selected correlation functions, $\gamma(r)$s, of the scattering data from *Figure 3*; the long periods L_C^Ms are indicated by arrows

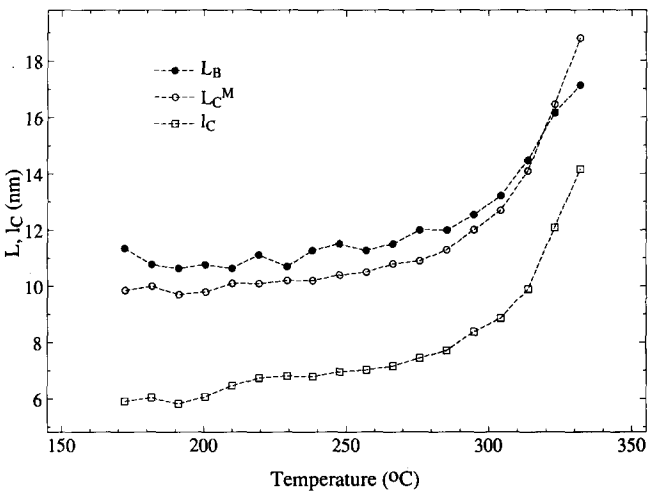

Figure 5 Variation, with temperature, of the two types of long period (L_B and L_C^M) and lamellar thickness l_C, using data obtained from *Figures 3* and *4*

that the case of multiple scattering maxima at 172°C *might* be real. In *Figure 3*, the peak position (q_{max}) first increased (172–191°C) and then decreased (191–332°C), with the increasing temperature. However, the scattering invariant (proportional to the area under the curve) continued to increase until the temperature exceeded 312°C (profile not shown). At 332°C, the invariant then decreased and the SAXS profile again showed an additional shoulder at high q (both the scattering maximum and the shoulder are indicated by arrows in the figure). Selected correlation functions, $\gamma(r)$, of the SAXS profiles from *Figure 3* are shown in *Figure 4*. The long period L_C^M was taken at the first maximum of $\gamma(r)$ (indicated by arrows), and was found to increase with temperature, as expected. In this figure, the deviation from linear behaviour as r approaches zero indicated the presence of a diffuse boundary between the crystalline and the amorphous regions. Therefore, the straight-line fit to $r=0$ yielded the invariant Q[20]. It was found that Q first increased with temperature until 312°C, and then decreased, as was also observed for the area under the Lorentz-corrected plot (see *Figure 3*).

The above scattering results are summarized in *Figures 5* and *6*. Two types of long period (L_B and L_C^M),

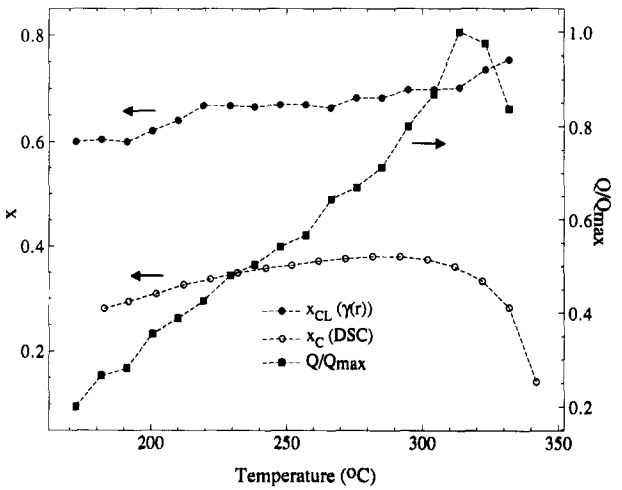

Figure 6 Variation, with temperature, of the normalized invariant Q/Q_{max}, the linear degree of crystallinity x_{CL} (determined from $\gamma(r)$) and the bulk-volume degree of crystallinity x_C (determined from *Figure 1* after density conversion)

determined using Bragg's law and $\gamma(r)$, are illustrated in *Figure 5*, which shows that L_B is usually larger than L_C^M. This phenomenon has been discussed before and was attributed to the broad distribution of both lamellar thickness and long period[1,16]. The temperature dependence of L_B was similar to that of L_C^M. Two regions of increase in the long period were seen, namely the first stage (below ~300°C) with a smaller increase, and the second stage (above 300°C) with a larger increase. The stage-transition temperature was found at ~300°C, which was also near the onset temperature of the melting endotherm in the d.s.c. studies. The normalized scattering invariant (defined as Q divided by the maximum invariant Q_{max}), determined from $\gamma(r)$ at different temperature, is shown in *Figure 6*. It was found that Q/Q_{max} increased linearly from 0.2 to 0.8 at temperatures from 172 to 292°C. Between 292 and 332°C, a maximum value was observed at ~312°C. The corresponding bulk-volume degree of crystallinity x_C, for the same heating rate, was estimated from the d.s.c. thermogram (*Figure 1*), using the following data; $\Delta H = 130\,J\,g^{-1}$ and $\rho_C = 1.4\,g\,cm^{-3}$ for 100% crystalline PEEK. It was seen that the value of x_C increased from 0.18 to 0.38 (approximately twofold) over the temperature range 172–282°C, while above 282°C, x_C started to decrease. The linear degree of crystallinity within the lamellar stacks, x_{CL}, estimated from $\gamma(r)$, is also shown in *Figure 6*. This estimation will be discussed below. It was found that x_{CL} increased consistently with temperature, from 0.6 (at 172°C) to 0.75 (at 332°C), with no sign of a maximum within the measured temperature range. The crystal lamellar thickness l_C, calculated as the product of L_C^M and x_{CL}, is also shown in *Figure 5*. It was seen that the value of l_C increased from 5.5 to 7.8 nm over the temperature range 172–332°C.

Isothermally crystallized specimens

Figure 7 shows d.s.c. scans (at a heating rate of $10°C\,min^{-1}$) of PEEK specimens crystallized at different temperatures (230–310°C). Typical double-melting behaviour can be seen there: a low melting temperature, T_{m_1}, always occurred at a temperature approximately 10°C above the crystallization temperature. The total heat of fusion was also found to increase slightly with increasing T_c.

Selected smoothed SAXS profiles (Iq^2 vs. q), measured at different temperatures for specimens crystallized at 260, 300, and 320°C, are shown in *Figures 8a–c*, respectively. Two features can be observed in these figures, i.e. the peak position q_{max} decreased with increasing temperature, and the area under the curves (proportional to Q) first increased with temperature, and then decreased at higher temperatures. Both features were also observed in the heating measurements carried out on amorphous samples (see above), except that the starting value of Q for the crystalline sample was approximately four times higher than that of the amorphous one. In *Figures 8a–c*, the 332°C SAXS profile consistently showed a scattering maximum at $0.35\,nm^{-1}$ and a secondary shoulder at $0.55\,nm^{-1}$. In fact, all seven specimens have shown a weak secondary scattering shoulder in the 332°C profiles, and these are illustrated in *Figure 9*. Since this temperature (332°C) was close to T_{m_2}, such SAXS profiles again indicated the presence of a heterogeneous lamellar arrangement during melting (with at least two types of long period identifiable by SAXS).

Bragg's law was used to calculate the values of the long period L_B for all seven specimens at different temperatures, and the results are shown in *Figure 10*. It was seen that L_B at a temperature of 142°C (i.e. below T_g) ranged from 13.5 to 16 nm for specimens crystallized over the range 260–320°C. These values were in good agreement with the previously published data obtained for quenched samples crystallized at similar temperatures[3,8]. Analogous to the behaviour illustrated in *Figure 5*, two stages of increase in L_B were observed. Each stage could be approximately described by a linear L_B *versus* temperature relationship, with the slope (L_B/T), in the first stage being significantly lower than that in

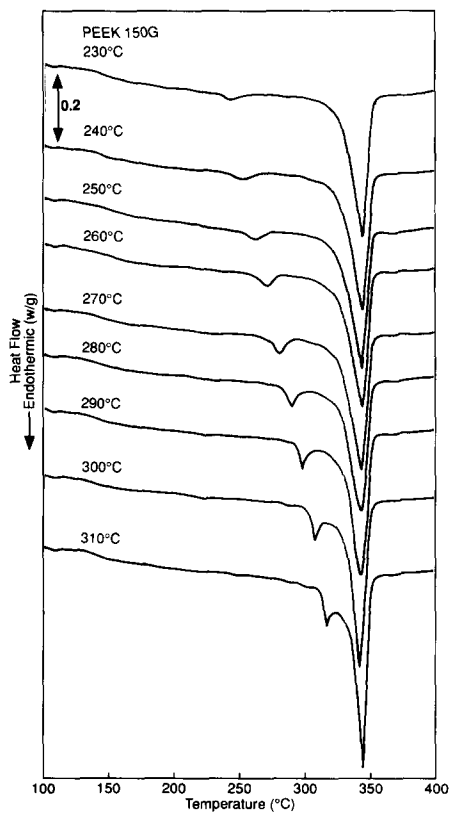

Figure 7 D.s.c. scans of isothermally crystallized PEEK specimens with different T_c values; the heating rate is $10°C\,min^{-1}$ in all cases

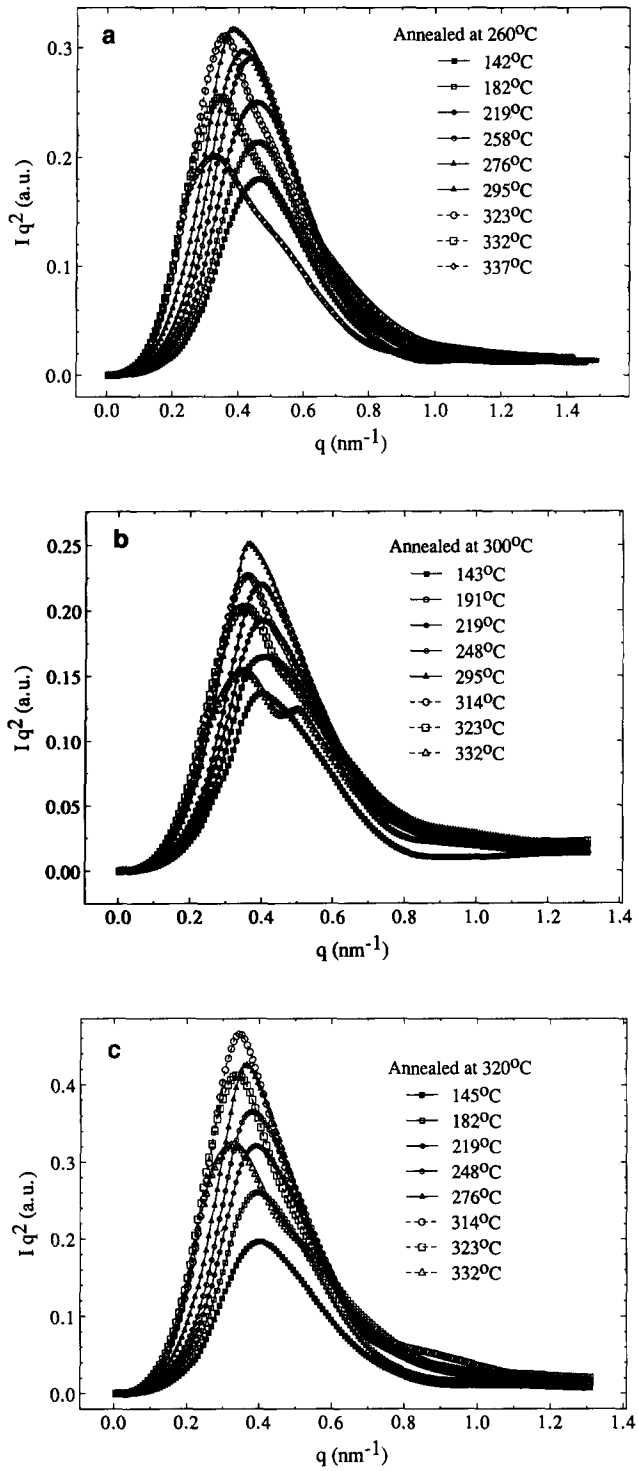

Figure 8 Selected Lorentz-corrected SAXS profiles of isothermally crystallized PEEK specimens with different T_c values: (a) 260; (b) 300 and; (c) 320°C. The heating rate is 10°C min^{-1} and the data collection time is 10 s

the second stage. A transition temperature was then defined as the intercept of the two lines of constant slope, which clearly increased with increasing crystallization temperature. This transition temperature was found to be near T_{m_1} in the d.s.c. scans. In addition, the ratio of L_B/T in the second stage decreased slightly with increasing crystallization temperature. As the temperature approached T_{m_2}, the L_B values of the different specimens appeared to converge on each other.

The values of the long period L_C^M determined from $\gamma(r)$ for all seven specimens, measured at different temperatures, are shown in *Figure 11*. A similar temperature dependence to that observed in *Figure 10* was also found with these results. Again, the increase in L_C^M showed a two-stage transition, with the transition temperature increased with increasing crystallization temperature. However, there were some differences

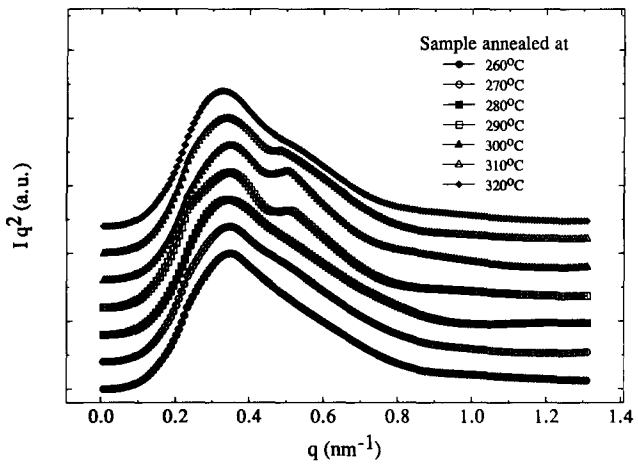

Figure 9 Lorentz-corrected SAXS profiles at 332°C for isothermally crystallized PEEK specimens with different T_c values

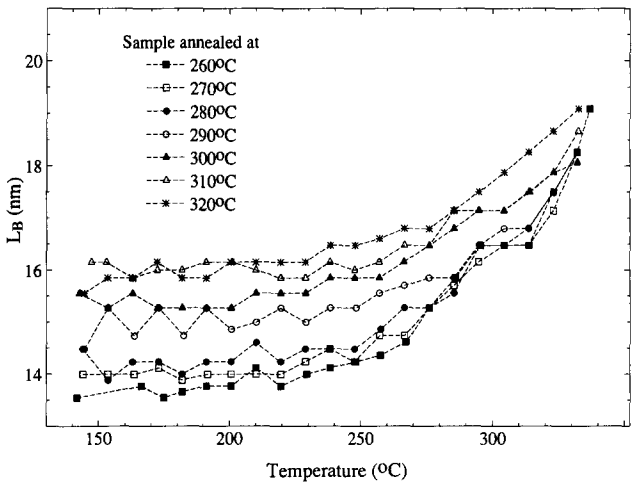

Figure 10 Variation, with temperature, of the long period L_B (determined by Bragg's law) for PEEK specimens with different T_c values

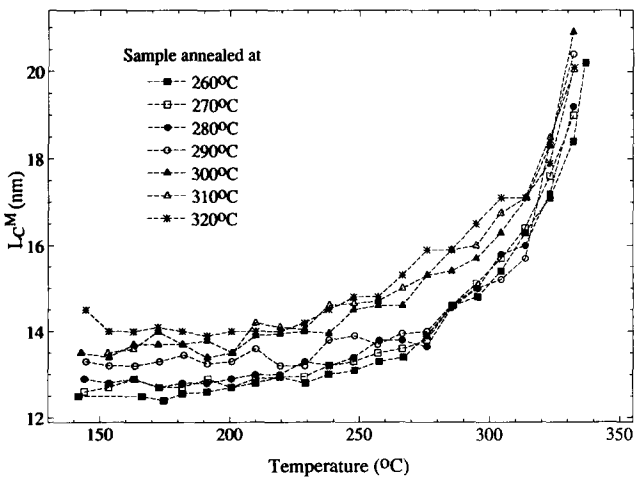

Figure 11 Variation, with temperature, of the long period L_M^C (determined from $\gamma(r)$) for PEEK specimens with different T_c values

between *Figures 10* and *11*. First, the starting value of L_C^M was lower than that of L_B, and secondly, the difference between the values of L_C^M for the different samples was smaller than that of the L_B values. At high temperatures (near T_{m_2}), the L_C^M values from the different samples were also found to converge on each other.

The normalized values of the invariant (Q/Q_{max}), determined from $\gamma(r)$ for different samples, are illustrated in *Figure 12* (curves are shifted vertically for comparison). It was seen that all curves showed a maximum between 302–322°C, and below 302°C, the value of Q/Q_{max} increased fairly linearly with temperature. The total increase in Q/Q_{max} from 142–302°C was less than 80%. Above 332°C, Q/Q_{max} began to decrease, but did not fall below the initial value, even at 332°C.

The corresponding linear degree of crystallinity x_{CL}, also determined from $\gamma(r)$, is shown in *Figure 13*. In this figure, x_{CL} was found to increase with temperature and covered the range from 0.6 to 0.8. This increase in x_{CL} became apparent only at temperatures above 222°C, which was near the maximum crystallization rate temperature (230°C). As pointed out before, the value of x_{CL} cannot be determined from $\gamma(r)$ alone[1,16]. The calculated x_{CL} values (0.6–0.8, with x_{CL} increasing with temperature) can be replaced by a second data set (0.4–0.2, with x_{CL} decreasing with temperature) and still satisfy the same mathematical equation (equation (3) in ref. 1). However, since the bulk-volume degree of crystallinity (x_C) for the crystalline specimens was usually about 0.35 at 280°C, the corresponding value of x_{CL} must be larger, or equal to this value ($x_C = 0.35$) in order to make physical sense. In other words, the volume fraction of the two-phase region, x_F ($= x_C/x_{CL}$), could be larger than unity (an impossible case), if $x_{CL} = 0.4$–0.2, and $x_C = 0.35$. Therefore, we concluded that x_{CL} had values in the range 0.6–0.8.

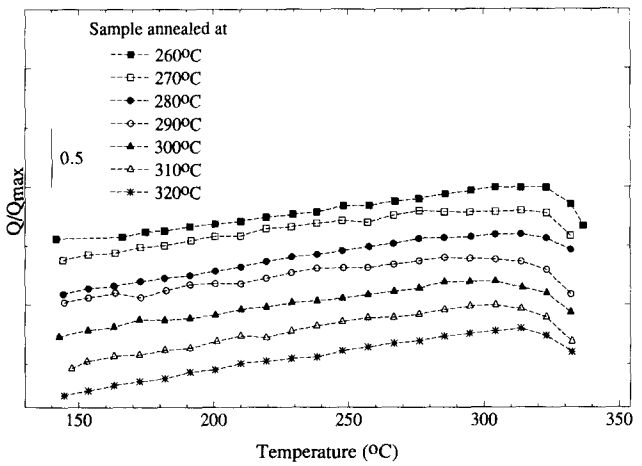

Figure 12 Variation, with temperature, of the normalized invariant Q/Q_{max} (determined from $\gamma(r)$) for PEEK specimens with different T_c values

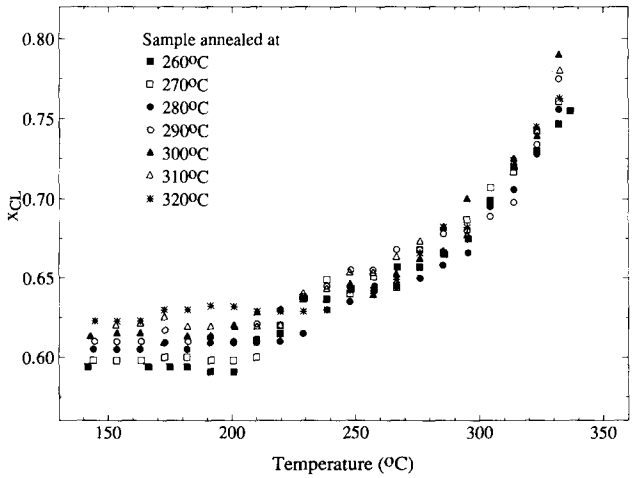

Figure 13 Variation, with temperature, of the linear degree of crystallinity within the lamellar stacks, x_{CL} (determined from $\gamma(r)$), for PEEK specimens with different T_c values

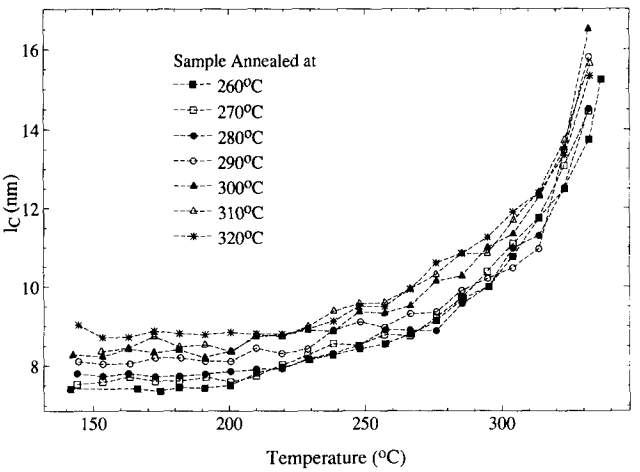

Figure 14 Variation, with temperature, of the lamellar thickness l_C, determined as the product of L_M^C and x_{CL}, for PEEK specimens with different T_c values

The values of the lamellar thickness l_C, calculated as the product of L_C^M and x_{CL}, are shown in *Figure 14*. It was seen that this thickness consistently increased with temperature, which was similar to the behaviour observed in the L_C^M *versus* temperature plot (*Figure 11*). The initial value of l_C (at 142°C) was found to increased with T_c. For example, specimens with T_c values from 260°C to 320°C showed values of l_C increasing from 7.5 to 9 nm, respectively. However, there was no correlation found between l_C and T_c at temperatures near T_{m_2}. At 332°C, the values of l_C showed a random scatter for the different specimens. However, the maximum value of l_C was found to be at the final measured temperature.

DISCUSSION

The multiple-peak feature of the SAXS profile at 172°C from the amorphous specimen (see *Figure 3*) *might* be real, despite the fact that the signal-to-noise ratio was low. One possible explanation is that during the cold crystallization (from the glassy state), the nucleation process is not only a function of time but is also a function of temperature. Consequently, the resulting morphology may consist of a broad population of lamellar thicknesses with several arrangements identifiable by SAXS. This argument is consistent with the persistent appearance of some weak secondary scattering shoulders in several other SAXS profiles (191–285°C).

Due to the complicated morphological nature of the cold crystallized specimen, we will first discuss the results from the isothermally crystallized samples, as the SAXS profiles for these were relatively straightforward. At temperatures below 332°C, a single scattering maximum was seen; only at 332°C, was there any indication of a dual-scattering maxima. In *Figures 10* and *11* (data

obtained from the primary scattering maximum), we found that both L_B and L_C^M increased with temperature in an 'upturn' two-stage fashion. Similar observations of increases in the long period (with the long period determined by Bragg's law) in crystalline samples have been made previously for several polymers, including PE, PET, PVDF/P3FE (60/40) and poly(aryl ether ketones)[2,21–24]. Keller first attributed this behaviour in PE to the melting of fine lamellae within the thicker lamellar stacking[21]. This model was also suitable for explaining our results and was modified slightly in the following way.

In our previous work, we have hypothesized that two types of lamellar stacks are formed during the isothermal crystallization; stacks with no lamellar insertion and stacks with two populations of lamellar thickness, as a consequence of the lamellar insertion (Figure 15 in ref. 1, similar to Keller's model). In this case, upon heating, the mean long period may change as follows. Before the melting of any crystallite, the long period can increase as a result of the thermal expansion of both the crystalline and amorphous components. This increase would be relatively small, which is consistent with the observation of the first-stage increase in L_B and L_C^M (see *Figures 10* and *11*). At temperatures above the melting point of the thinner lamellae, these lamellae will be melted away, leaving behind the thicker lamellae in the stacks (as illustrated in *Figure 15*). This would result in a progressive increase in the mean long period, which also agrees with the observation of the larger, second-stage increase. Moreover, the latter process could produce two types of lamellar stacks with similar lamellar thicknesses, but with a different long period (Figure 15 in ref. 1), which is also consistent with the appearance of a weak secondary scattering shoulder found in the SAXS profiles at 332°C (*Figure 9*).

Bassett *et al.* first used the dual-lamellar thickness model to explain the double-melting behaviour in PEEK[7]. In this work, we found further evidence to support this model. A good agreement was found between the lower melting temperature T_{m_l} and the stage-transition temperature of the long period increase (such as L_B), which indicated that T_{m_l} might indeed represent the melting of thinner secondary lamellae. In this case, the thickness of the secondary lamellae must increase with T_c, as seen by the double-melting behaviour in d.s.c. measurements. This may be understood by the following argument. A simultaneous increase in the interlamellar amorphous spacing is expected at higher values of T_c, which allows for the growth of thicker secondary lamellae. Recently, Krüger and Zachmann have investigated the multiple-melting endotherms induced by step-annealing in related systems of poly(aryl ether ketones), including PEEKK, PEKEKK and PEEK, using simultaneous SAXS/WAXD and thermal analysis[23]. They also found that the long period (determined by Bragg's law) increased with temperature in a step-like fashion, with the step-transition temperature similar to the melting temperature of the lower endotherms. This again supports the hypothesis that the annealing-induced endotherm is due to the melting of thin secondary lamellae within the lamellar stacks. Although our results support the suggestion that the double-melting behaviour is due to the melting of two distinct morphologies, evidence of recrystallization, at least in the form of lamellar thickening, was also observed (see *Figure 14*). The recrystallization process was the core argument for the second hypothesis, which attributed the double-melting behaviour merely to the melting and recrystallization of the primary crystal morphology. Perhaps, a compromised view between the two hypotheses can be proposed, i.e. the lower-temperature endotherm is due to the melting of thinner secondary lamellae within the lamellar stacks, whereas the higher-temperature endotherm represents the melting of primary lamellae after being thickened. Consequently, the latter process does not represent the melting of the original morphology, but the former process does.

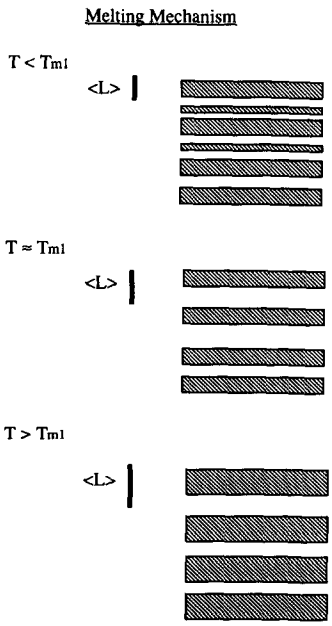

Figure 15 Schematic representation of the melting mechanism for the dual-lamellar thickness model; the thinner shaded bars represent the secondary lamellae and the thicker ones represent the primary lamellae which are subsequently thickened

It is known that Q can be expressed as[1,16]:

$$Q = Cx_F x_{CL}(1-x_{CL})(b_C-b_A)^2 = Cx_C(1-x_{CL})(b_C-b_A)^2 \quad (2)$$

where C is a constant and $(b_C-b_A)^2$ is the electron-density contrast between crystalline and amorphous components. In *Figure 12*, it was seen that Q/Q_{max} increased by about 80% from 142 to 302°C for all of the specimens. However, the corresponding x_C value (as determined by the heat of fusion in *Figure 7*) was found to decrease slightly, due to the melting of the lower endotherm, while x_{CL} increased from 0.6 to 0.7 (*Figure 13*). Both of these two terms would decrease the value of Q/Q_{max}, according to equation (2). Therefore, the increase in Q/Q_{max} must be largely attributed to the increase in the electron-density contrast, $(b_C-b_A)^2$. This is quite a reasonable conclusion because the thermal expansion coefficients of the crystalline and amorphous components are very different for PEEK. In this case, the value of $(b_C-b_A)^2$ was found to increase with temperature. At temperatures above 312°C, the value of Q/Q_{max} was found to decrease, and this could be attributed to a combination of an increase in x_{CL} (*Figure 13*) and a decrease in x_F. The latter decrease was apparent, since the value of x_C was also decreased over this temperature range.

For the cold crystallized specimen (originally amorphous), different results were observed. First, d.s.c.

measurements showed an exotherm, but no indication of the double-melting behaviour (*Figure 1*). Secondly, a stage-transition temperature in the long period was observed at approximately 300°C, which was near the onset temperature of the final endotherm (*Figure 1*). Thirdly, the long period in the first stage was found to be lower than that of the isothermally crystallized specimen, but the increase in Q/Q_{max} (about 400% in *Figure 6*) was found to be larger. The appearance of the exotherm indicated that the heating process was not a straightforward melting phenomenon but a combination of crystallization and melting. The cold crystallization is probably responsible for the above differences, which can be explained as follows. Since the majority of the cold crystallization process took place at approximately 170°C, it is understood that the resulting long period would be lower than that produced at higher temperatures, as in the case of isothermally crystallized specimens. However, the broad cold crystallization (165–280°C) probably generated a wide distribution of lamellar thicknesses, which could be partially contributed by the lamellar insertion mechanism, thus resulting in a decrease in the long period. This mechanism should somewhat offset opposing effects such as thermal expansion and the melting of thin secondary lamellae, both of which would increase the long period, and thus result in a higher stage-transition temperature (at about 300°C). In the case of the large increase in Q/Q_{max}, we believe that this is due to two separate effects; the thermal expansion, as discussed earlier, and the increase in the bulk-volume degree of crystallinity, x_C, from the cold crystallization process, with the later effect probably being the more dominant one.

CONCLUSIONS

In this work, we have determined both L_B and L_C^M, the invariant ratio Q/Q_{max}, and the lamellar thickness l_C, over a range of temperatures, during the heating of amorphous and isothermally crystallized samples, using time-resolved synchrotron SAXS. In the isothermally crystallized specimens, L_B and L_C^M increased with temperature in two stages, namely a smaller increase at lower temperatures and a larger increase at higher temperatures. The stage-transition temperature was found near the peak temperature of the lower endotherm, T_{m_l}, in d.s.c. measurements. It was also seen that Q/Q_{max} increased with temperature and showed a maximum above 300°C, whereas l_C increased throughout the entire measured temperature range (to 332°C). In addition, a secondary scattering shoulder was consistently observed at 332°C for all of the crystalline samples. These results were explained by a dual-lamellar thickness model, first proposed by Keller[21], and later by Bassett *et al.*[7]. According to this model, the lower endotherm observed in the d.s.c. measurements was attributed to the melting of the thinner secondary lamellae within the lamellar stacks. Consequently, below T_{m_l}, the smaller increase in the long period was attributed to the thermal expansion (as was the increase in Q/Q_{max}); above T_{m_l}, the larger increase in the long period was due to the melting away of the thinner secondary lamellae. In contrast, the higher endotherm observed in the d.s.c. measurements was attributed to the melting of the residual primary lamellae after being thickened. In the amorphous sample, the scattering results were dominated by the presence of the broad cold crystallization. As a result, several unique features were observed, which included a lower mean value for the initial long period, a higher stage-transition temperature near the onset temperature of the final endotherm, and a larger increase in Q/Q_{max}.

ACKNOWLEDGEMENTS

The authors wish to thank J. P. McKeown and Y. J. Li for their assistance with the synchrotron experiments, and Dr M. Keating and R. M. Koveleski for the thermal analysis measurements. Discussions with Dr H. G. Zachmann were most helpful in the preparation of this work.

REFERENCES

1 Hsiao, B. S., Gardner, K. H., Wu, D. Q. and Chu. B. *Polymer* 1993, **34**, 3986
2 Bark, M., Schulze, C. and Zachmann, H. G. *Am. Chem. Soc. Div. Polym. Chem. Polym. Prepr.* 1991, **31**, 106
3 Blundell, D. J. and Osborn, B. N. *Polymer* 1983, **24**, 953
4 Cebe, P. and Hong, S. D. *Polymer* 1986, **27**, 1183
5 Lee, Y. and Porter, R. S. *Macromolecules* 1987, **20**, 1336
6 Blundell, D. J. *Polymer* 1987, **28**, 2248
7 Bassett, D. C., Olley, R. H. and Al Raheil, I. A. M. *Polymer* 1988, **29**, 1945
8 Lee, Y., Porter, R. S. and Lin, J. S. *Macromolecules* 1989, **22**, 1756
9 Bell, J. P. and Murayama, T. *J. Polym. Sci. (A-2)* 1969, **7**, 1059
10 Roberts, R. C. *Polymer* 1969, **10**, 117
11 Yeh, J. T. and Runt, J. *J. Polym. Sci., Polym. Phys. Edn* 1989, **27**, 1543
12 Gardner, K. H., Hsiao, B. S., Matheson, R. R. and Wood, B. A. *Polymer* 1992, **33**, 2483
13 Cheng, S. Z. D., Cao, M. Y. and Wunderlich, B. *Macromolecules* 1986, **19**, 1868
14 Zachmann, H. G. and Stuart, H. A. *Makromol. Chem.* 1960, **41**, 148
15 Holdsworth, P. J. and Turner-Jones, A. *Polymer* 1970, **12**, 195
16 Santa-Cruz, C., Stribeck, N., Zachmann, H. G. and Baltá-Calleja, F. J. *Macromolecules* 1991, **24**, 5980
17 Song, H. H., Stein, R. S., Wu, D. Q., Ree, M., Phillips, J. C., LeGrand, A. and Chu, B. *Macromolecules* 1988, **21**, 1180
18 Song, H. H., Wu, D. Q., Chu, B., Satkowski, M., Ree, M., Stein, R. S. and Phillips, J. C. *Macromolecules* 1990, **23**, 2380
19 Chu, B., Wu, D. Q. and Howard, R. *Rev. Sci. Instrum.* 1989, **60**, 3224
20 Rudland, W. *Colloid Polym. Sci.* 1977, **255**, 417
21 Keller, A. IUPAC Int. Symp., Macromol. Proc., Florence, 1980, p. 135
22 Lopez-Cabarcos, E., Gonzalez-Arche, A., Baltá-Calleja, F. J., Bösecke, P., Röber, S., Bark, M. and Zachmann, H. G. *Polymer* 1991, **32**, 3097
23 Krüger, K. N. and Zachmann, H. G. *Macromolecules* in press
24 Wang, J., Alvarez, M., Zhang, W., Wu, Z., Li, Y. and Chu, B. *Macromolecules* 1992, **25**, 6943